

Application of singular value decomposition analysis to time-dependent powder diffraction data of an *in-situ* photodimerization reaction

Ahmed F. Mabied,^{a,*} Shunsuke Nozawa,^b Manabu Hoshino,^{c,d} Ayana Tomita,^b Tokushi Sato^b and Shin-ichi Adachi^{b,e,f}

^aX-ray Crystallography Laboratory, Solid State Department, Physics Division, National Research Center, El Buhouth (El-Tahrir) Street, Dokki, Giza 12622, Egypt, ^bPhoton Factory, High Energy Accelerator Research Organization, KEK, Tsukuba 305-0801, Japan, ^cDepartment of Chemistry and Materials Science, Tokyo Institute of Technology, Meguro-ku, Japan, ^dCREST, Japan Science and Technology Agency, Japan, ^eDepartment of Materials Structure Science, School of High Energy Accelerator Science, KEK, The Graduate University for Advanced Studies, Sokendai, Tsukuba 305-0801, Japan, and ^fPRESTO, Japan Science and Technology Agency, Japan. E-mail: mabied@xrldlab-nrc-eg.org

Singular value decomposition (SVD) analysis has important applications for time-dependent crystallographic data, extracting significant information. Herein, a successful application of SVD analysis of time-resolved powder diffraction data over the course of an *in-situ* photodimerization reaction of anthracene derivatives is introduced. SVD revealed significant results in the case of 9-methylanthracene and 1-chloroanthracene. The results support the formation of the 9-methylanthracene stable dimer phase and suggest the existence of an excimer state.

Keywords: singular value decomposition; anthracene derivatives; photodimerization; time-dependent; X-ray powder diffraction.

1. Introduction

The rapid development of time-resolved X-ray experiments has raised challenges regarding data analysis and the extraction of significant information. Singular value decomposition (SVD) analysis introduces an excellent solution, where large data sets containing a number of values can be reduced to fewer data sets containing significant values while conserving the correlation of variables of the original data. SVD is able to decompose time-resolved data into time-independent and time-dependent components. Also, it can help to extract meaningful signals from noisy data (Henry & Hofrichter, 1992; Rajagopal *et al.*, 2004).

SVD analysis has had a variety of successful applications in crystallography; for instance, with time-resolved small-angle X-ray scattering (Okamoto & Sakurai, 2003) and time-resolved macromolecular crystallographic data (Zhao & Schmidt, 2009; Rajagopal *et al.*, 2004). In addition, it has been successful in many other areas such as spectroscopy (Berlich *et al.*, 2005; Henry & Hofrichter, 1992; Henry, 1997), gene expression data (Alter *et al.*, 2000; Wall *et al.*, 2003), scientific computing and signal processing (Lahabar & Narayanan, 2009). Among these applications, SVD has proved efficient in treating time-dependent crystallographic and spectroscopic data. It can reveal important information by extracting small changes from the data that could not be detected directly

(Oka *et al.*, 2000; Rajagopal *et al.*, 2004; Zhao & Schmidt, 2009; Henry & Hofrichter, 1992).

The present study sheds some light on the advantages of applying SVD analysis to time-resolved crystallographic data in the case of powder diffraction. The target here is to treat the data of *in-situ* photodimerization time-dependent powder diffraction measurements of the anthracene derivatives 1-chloroanthracene (1-chA) and 9-methylanthracene (9-MA).

Upon illumination with light of wavelength >300 nm, anthracene derivatives undergo important photodimerization to form a stable dimer phase, which can be dissociated into its initial monomers either thermally or by illumination under light of wavelength <300 nm (Bouas-Laurent *et al.*, 2001; Schmidt, 1971). Based on their photodimerization properties, many applications have been developed, such as the fabrication of photo-switchable devices (Zhao *et al.*, 2008), control of biological reactions (Molard *et al.*, 2006) and with optical storage memory devices (Dvornikov & Rentzepis, 1996).

Reported possible processes during monomer–dimer transformations due to the photoreaction are as follows: monomers absorb the light ($2M + h\nu \rightarrow M^*$) and then relax to instantly excited monomers (M^{ex} , excimer). The excimer could either disintegrate into stable monomers ($M^{ex} \rightarrow 2M + h\nu$) or form a stable dimer ($M^{ex} \rightarrow D$). However, forming the excimer is faster than forming a stable dimer (Takegoshi *et al.*, 1998; Ferguson & Mau, 1974). Moreover, Aladekomo (1973)

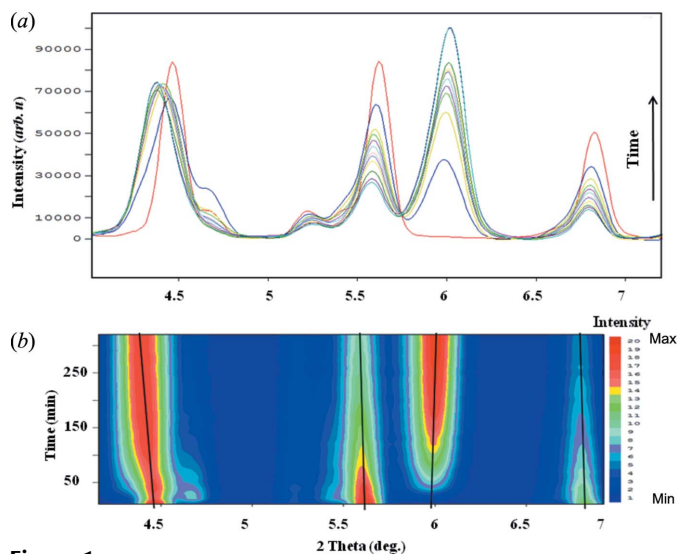


Figure 1 Time-resolved powder diffraction profiles of 9-MA photodimerization showing the deviations with 2θ . (a) Raw data. (b) Two-dimensional contour plot.

reported that 9-MA is one of the unique materials which enables the study of excimer and stable dimer.

In our previously reported photodimerization study of 9-MA (Mabied *et al.*, 2012), the time-dependent powder diffraction data of 9-MA monomer and dimer phases were analyzed quantitatively based on the averaged structure in each phase. The study overcomes the drawbacks of photo-reactions in a single crystal by the application of powder diffraction reaching higher completion (63.8%) of the dimer fraction. The suggested phase-transition kinetics reveal that small parts of the reactant phase (nuclei of the dimer) appear randomly in the parent phase at the beginning of the reaction. This means that the dimer and its associated excimer state should exist. In addition, it could enhance the change of the averaged diffraction intensity in the monomer phase despite the dimer peaks not yet having appeared, as shown in Figs. 1 and 2. Therefore, the aim of this study is to find any traces of the excimer state by applying SVD analysis, which could not be observed directly using Rietveld refinement.

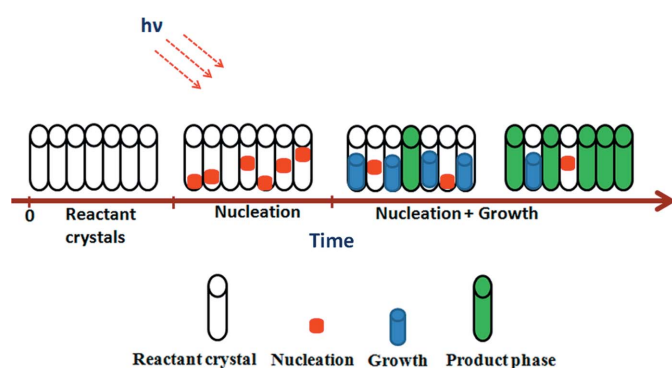


Figure 2 Schematic diagram of the 9-MA solid-state ($4\pi+4\pi$) photodimerization kinetics.

2. Experimental

1-Chloroanthracene powder (95% pure) was obtained from Sigma Aldrich Company and 9-methylanthracene (98% pure) was supplied by Wako Chemical Co., Japan. All the samples were ground using an agate mortar and pestle after recrystallization from acetone and hexane solvents. The samples were filled into borosilicate glass capillaries of diameter 0.4 mm (Hilgenberg, Germany).

The photodimerization experiment was carried out *in-situ* at the X-ray time-resolved beamline NW14A of the Photon Factory Advanced Ring (PF-AR) facility, KEK, Japan. Details of the beamline are given elsewhere (Nozawa *et al.*, 2007). The X-ray beam was set to an energy of 18.0 keV ($\lambda = 0.689 \text{ \AA}$). The samples were mounted on a horizontal φ -axis and rotated around this axis for better counting statistics. The sample-to-detector distance was set as 150 mm and calibrated using the 111 diffraction ring from standard silicone powder. Powder diffraction rings were collected at ambient temperature, which was about 302 K at the sample position, using a Mar165 CCD detector. Visible light from a xenon lamp with a visible mirror module (MAX-301; 385–740 nm, 300 W; Asahi Spectra) illuminated the sample undergoing photodimerization during data collection. IR spectra were measured on a Shimadzu IR Prestige-21 FTIR spectrometer by dispersing samples in KBr pellets. UV–Vis absorption spectra were recorded using a Varian Cary 50 Conc spectrophotometer in a cyclohexane solution.

3. SVD and data treatment

3.1. SVD

Mathematically, singular value decomposition can be defined as follows. An m -by- n real matrix A ($m \geq n$) can be decomposed into three matrices U , S and V^T [$A_{m,n} = USV^T$, equation (1)]. U is an m -by- n ($m \geq n$) matrix having the property that $U^T U = I_n$, where I_n is the identity matrix; columns of U are called the left singular vectors of A . The matrix S is an n -by- n diagonal matrix with non-zero elements in descending order ($s_1 \geq s_2 \geq \dots \geq s_n \geq 0$) and called the singular values of A , which also indicates the matrix rank. V^T is the transpose of an n -by- n matrix V ($V^T V = I_n$), where I_n is the identity matrix; columns of V are called the right singular vectors of A . Further details can be found elsewhere (Henry & Hofrichter, 1992; Stoer & Bulirsch, 2002; Unonius & Paatero, 1990; Golub & Van Loan, 1996).

$$A_{m,n} = \begin{pmatrix} u_{1,1} & \cdots & u_{1,n} \\ \vdots & \ddots & \vdots \\ u_{m,1} & \cdots & u_{m,n} \end{pmatrix} \begin{pmatrix} s_1 & & \\ & \ddots & \\ & & s_n \end{pmatrix} \begin{pmatrix} v_1 & \cdots & v_{1,n} \\ \vdots & \ddots & \vdots \\ v_{n,1} & \cdots & v_{n,n} \end{pmatrix} \quad (1)$$

Physically, according to the literature (Henry & Hofrichter, 1992; Unonius & Paatero, 1990), the SVD method can factorize an experimental data m -by- n matrix into several components matrices. The columns of the U matrix represent the measurements base spectrum of the original data and the S

elements give its singular values, which indicate the importance of the U spectrum. The singular values are arranged in descending order according to their magnitudes. The V matrix gives the associated time-dependent vectors of the U elements. In other words, based on the obtained singular values (s_1, \dots, s_n) and the characteristics of the U spectrum, the importance of the U columns (u_1, \dots, u_n) is decided, and hence the associated time-dependent vectors of V (v_1, \dots, v_n) can be fitted (Henry & Hofrichter, 1992; Unonius & Paatero, 1990). The SVD results can be interpreted successfully based on global fitting of the column vectors of the

matrix V extraction of time-independent correlations (Zhang *et al.*, 2004; Van Wilderen *et al.*, 2011; Henry & Hofrichter, 1992; Unonius & Paatero, 1990). Visualization of the singular values is the most important step for understanding the results of the U , S and V matrices and to decide the meaningful components. One of the graphical methods used is a one-dimensional plot, where the height of any one singular value is indicative of its importance in explaining the data. The relative variances [$s_n^2(\sum_i s_i^2)^{-1}$] are often plotted, where the square of each singular value is proportional to the variance explained by each singular vector. These kinds of plots are called scree plots, as referred to by Cattell (Cattell, 1966; Wall *et al.*, 2003).

3.2. Data treatment

The standard 2θ versus intensity powder diffraction patterns through the measurement time were obtained from the recorded powder diffraction rings using *Fit2D* (Hammersley *et al.*, 1996). The geometrical correction was applied and the beam center shadows and contamination spots were masked (Hammersley *et al.*, 1996). For more accuracy, the background was subtracted from the data using *Powder3D* software (Hinrichsen *et al.*, 2006) before SVD analysis. *WinPLOTR* (Roissnel & Rodriguez-Carvajal, 2001) and *Powder3D* (Hinrichsen *et al.*, 2006) were used to visualize the time-resolved data.¹

The corrected powder data were set into an m -by- n matrix, where the columns are the diffraction intensity at the 2θ angle points (Fig. 3) [for further reading about data treatment, see Henry & Hofrichter (1992) and Oka *et al.* (2000)].

The SVD was computed according to the reported procedures, where the data matrix A can be described by an m -by- n matrix $P(2\theta)$ and an n -by- n matrix $C(t)$ as $A(s, t) = P(2\theta)C(t) = USVT$. Here, $P(2\theta)$ and $C(t)$ represent the diffraction pattern of the independent components and their concentrations as a function of time t , respectively. As mentioned above, U contains the basis spectra of the diffraction pattern, S contains

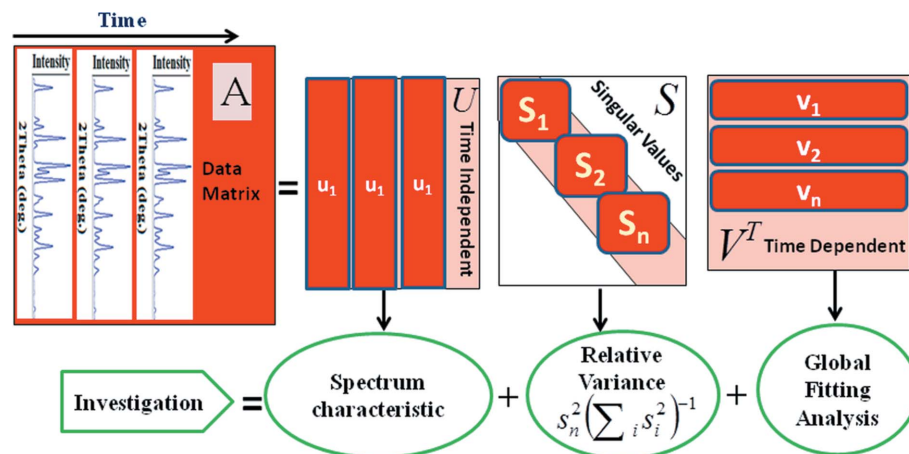


Figure 3 Schematic diagram showing how SVD works with time-resolved X-ray powder diffraction data.

the associated eigenvalues, and V contains the time-dependence of the basis spectra.

The statistical weights for the data set \mathbf{A} have been considered. The weight matrix W is defined as $W_{ij} = 1/\sigma_{ij}$ ($i = j$) and $W_{ij} = 0$ ($i \neq j$), where the error of the data element $A(2\theta_i, t_j)$ is described as σ_{ij} . Since the measurement time is identical for all data, the error would depend on 2θ . The value of σ_{ij} is given as the average of the square root of A_{ij} for all frames ($j = 1$ to n). Therefore, the final data set to be analyzed should be $WA = USVT = WU'SVT$, where $U' = B^{-1}U$. Then, $A = U'SV^T$.

The matrix dimensions were (1233, 59) and (1095, 42) for 9-MA and 1-chA, respectively. According to ($A = U'SV^T$), the SVD was calculated and produced the three matrices U , S and V . The results (see §4) of the time-dependent spectra of the V matrix were plotted. Fitting analysis of the V curves showed the best fit function for the double exponential function [equation (2)]. As the results do not correspond directly to independent states in the photoreaction, the diffraction profiles need to be reconstituted. Global fitting analysis can extract the time-independent correlations and their associated rate constants. Therefore, it was applied to the 9-MA data. The parameters of equation (2) have been obtained successfully and can be defined as follows: A_0 is a time-independent part, which should be unchanged during the photoreaction. A_1 and A_2 are the changing parts; their rate constants are k_1 and k_2 , respectively. The powder diffraction profile during the photoreaction can be considered as a summation of all these profiles A_0 , A_1 and A_2 . All SVD calculations and fitting were performed using *IGORPro* (Wave Metrics, 2011),

$$F(t) = A_0 + A_1 \exp(-k_1 t) + A_2 \exp(-k_2 t). \quad (2)$$

4. Results and discussion

SVD analysis of the present data gives the three matrices U , S and V . Investigation of the results can be considered as an aggregate of three major steps (Fig. 3): the first is determining the important singular values from the S matrix using a

¹ Raw X-ray diffraction data of both 9-MA and 1-chA are available from the IUCr electronic archives (Reference: CO5048).

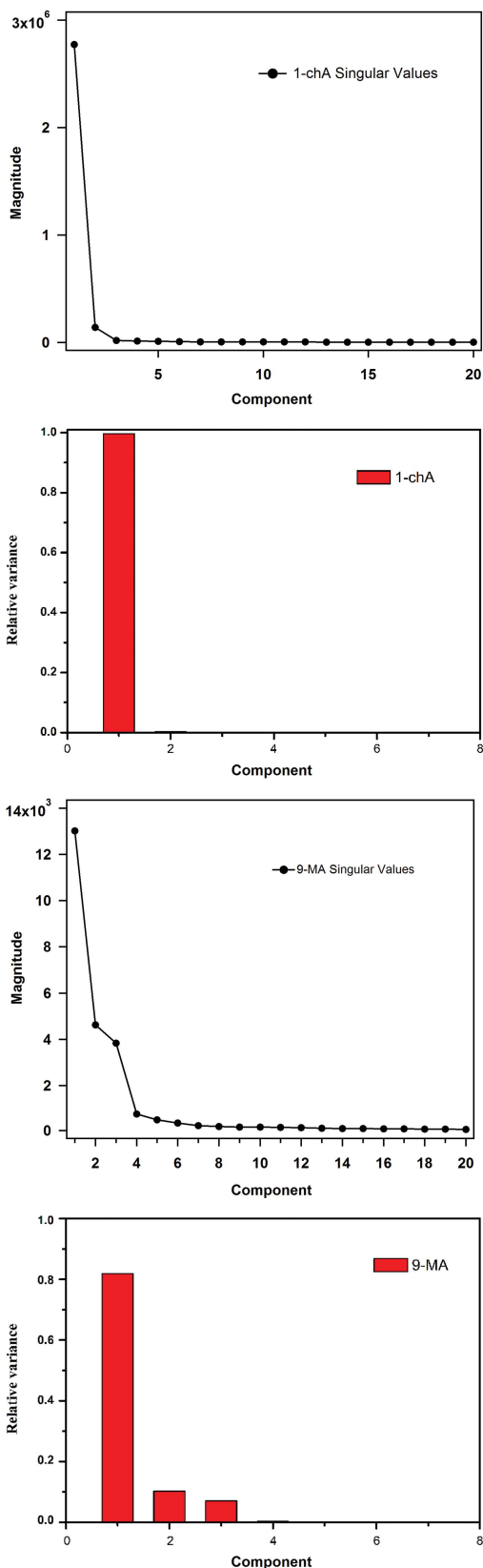


Figure 4
Comparison of the resultant singular values of SVD analysis of time-resolved powder diffraction data of both 9-MA and 1-chA data, illustrating the singular values *versus* their components of the obtained *S* matrix and the relative variance plot (red bars) showing the importance of each component.

visualization method (such as relative variance); the second is checking the associated base spectrum characteristics of the matrix *U*; and the third is examining the behaviour of the time-dependent vectors of the matrix *V* using global fitting analysis.

Fig. 4 shows a comparison of the resultant singular values of the 9-MA and 1-chA data. It illustrates the singular values *versus* their data components of the obtained *S* matrix. The importance of every component is indicated by the relative variance plot (red bars). The significance was decided based on the visualized singular values and their distinctive *U* and *V* spectra.

For 1-chA data, there is a distinguishable singular value component ($s_1 = 2.8 \times 10^6$) and relatively smaller s_2 component, as shown in Fig. 4. The s_1 -related v_1 spectrum shows almost time-independency (Fig. 5). The associated u_1 spectrum characteristics are similar to the original diffraction pattern of the 1-chA monomer phase (Fig. 6).

Fig. 7 shows that there is almost no change in the position of the peaks of the 1-chA diffraction pattern during the illumination in contrast to 9-MA (Fig. 1). This indicates that the photodimerization of 1-chA barely proceeded. The consistency of IR and UV-Vis spectra under the photoirradiation condition (Fig. 8) ensured less activity of this reaction. However, v_2 showed time-dependency (Fig. 5): the best curve fitting matched the double exponential function [equation (2)], which gave fast behaviour only with almost the same rate constant ($k_1 = 3.148 \pm 0.093 \times 10^{-5} \text{ s}^{-1}$ and $k_2 = 3.1 \pm 0.093 \times 10^{-5} \text{ s}^{-1}$) in contrast to the case of 9-MA, as shown in Table 1.

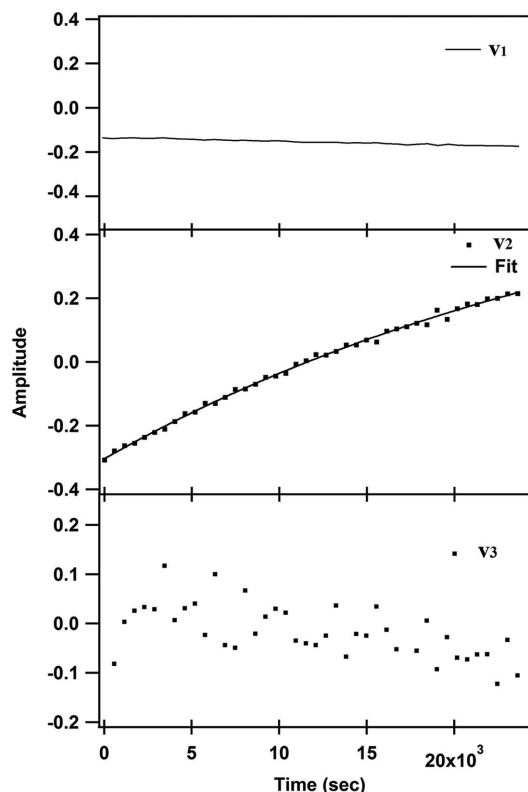


Figure 5
The first three significant amplitude vectors of *V*, associated with the singular values obtained from SVD analysis of 1-chA data.

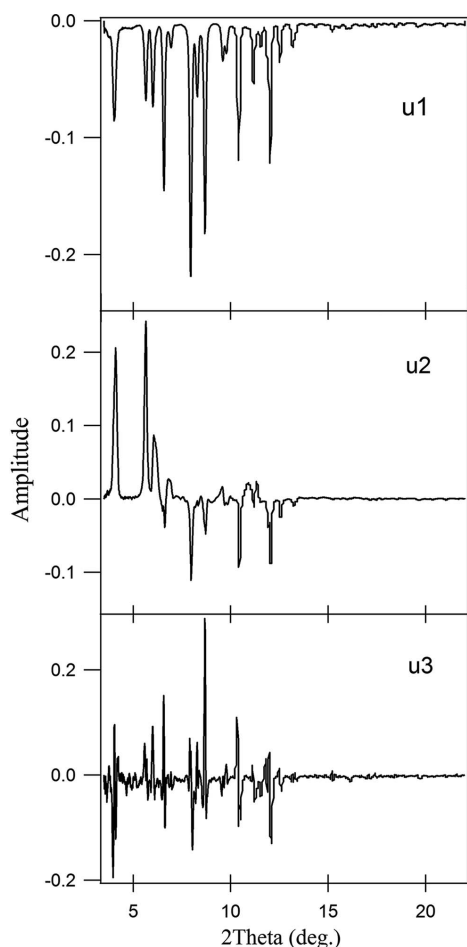


Figure 6
 U spectra (u_1 , u_2 and u_3) associated with the first three singular values of 1-chA.

The existence of such time-dependency character, even if the dimer phase does not appear, could suggest that it is coming from the excimer state, which can disintegrate into the stable monomers without forming the dimer phase of 1-chA. This is in agreement with the reported possible paths of the photo-dimerization reaction as mentioned in the *Introduction*.

The visualization of the 9-MA data singular values (Fig. 4) indicates that three components are significant. The first three singular values ($s_1 = 13021.54$, $s_2 = 4620.65$ and $s_3 = 3835$) are

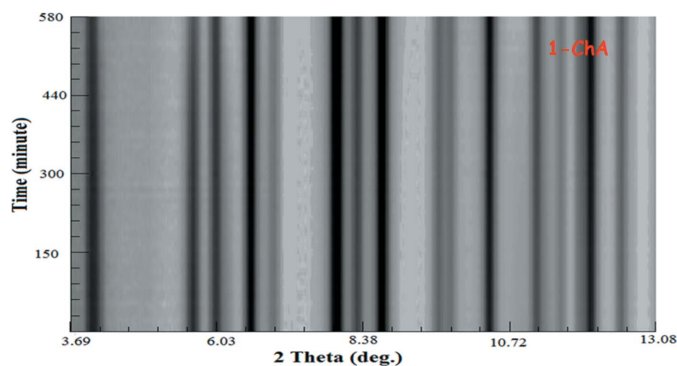


Figure 7
 Waterfall presentation of the propagation of typical Bragg diffraction peaks of 1-chA.

larger than the other values and give the non-random U spectrum (Fig. 9), which could point out that the higher singular values come from noise. The accompanying u_1 , u_2 and u_3 (Fig. 9) spectra and their time courses v_1 , v_2 and v_3 (Fig. 10) can give information about this significance.

However, the first component (s_1) is the largest one. The distinct u_1 spectrum was similar to the diffraction pattern of the 9-MA dimer phase (Fig. 1) except for its negative sign (Fig. 9), which corresponds to the sign of v_1 (Fig. 10). Oka *et al.* (2000) have reported similar cases. v_1 showed little time-dependency at the lower values, as noticeable in Fig. 10; the character of v_1 arises from the existence of the stable dimer.

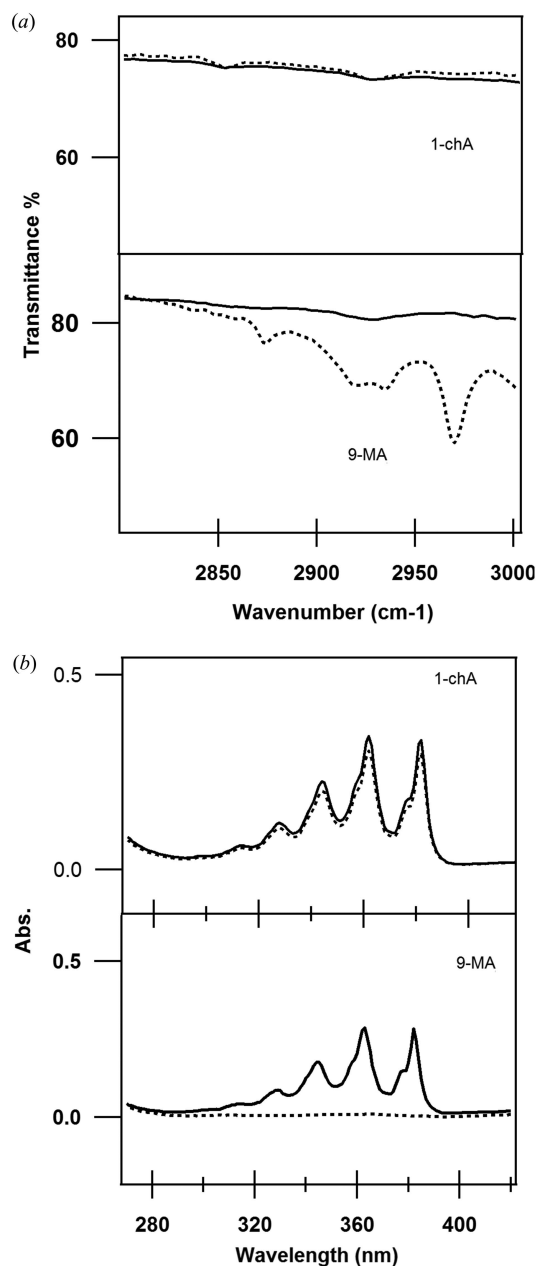


Figure 8
 Selected bands of the measured spectra of 9-MA and 1-chA. The dotted lines, representing the illuminated samples, show that there is no change in the case of 1-chA, contrary to 9-MA. (a) IR spectra. (b) UV-Vis spectra.

The other two components u_2 and u_3 are also significant because of their distinct u_2 and u_3 spectra, which are distinguishable from noise.

The first V spectrum (v_1) was almost time-independent during the measurement, while the second spectrum (v_2) was seen to decay and the third (v_3) to grow, as shown in Fig. 10. This means that, even if the amount of one component decreased, another component increased to compensate for the decrease in the diffraction intensity. This is consistent with similar cases (Okamoto & Sakurai, 2003).

The characteristics of the U spectrum support this assumption, where the u_2 and u_3 spectra look like a diffraction pattern composed of diffraction peaks of the 9-MA monomer and dimer phases (Figs. 1 and 9) while neglecting the peak directions. The associated v_2 and v_3 spectra showed notable

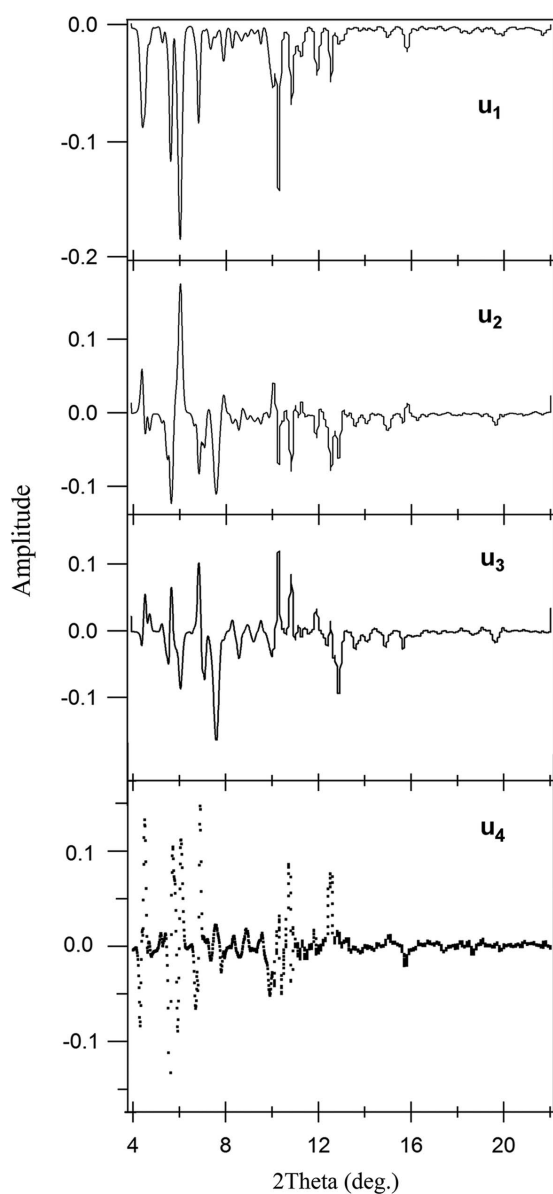


Figure 9
 U spectra (u_1 , u_2 , u_3 and u_4) associated with the first four singular values $s_1 = 13021.54$, $s_2 = 4620.65$, $s_3 = 3835$ and $s_4 = 762.241$ for SVD analysis of the 9-MA data.

Table 1
Global fitting result of 9-MA data showing parameters of equation (2).

	A_0 (constant)	A_1 ($k_1 = 6.8 \pm 0.3 \times 10^{-5} \text{ s}^{-1}$)	A_2 ($k_2 = 109.0 \pm 0.90 \times 10^{-5} \text{ s}^{-1}$)
v_1	-0.1357 ± 0.0007		
v_2	0.1604 ± 0.0055	-0.3488 ± 0.0047	-0.1793 ± 0.0086
v_3	-0.1029 ± 0.0042	0.2588 ± 0.0046	0.1520 ± 0.0079

time-dependency in contrast to the v_1 spectrum (Fig. 10). The v_2 and v_3 spectra were fitted successfully with a double exponential function [equation (2)] using global fitting analysis (Fig. 10). The results of the global fitting analysis are given in Table 1. For simplicity, it can be imagined roughly that the X-ray diffraction profile is a summation of all three profiles that do not correspond directly to the independent states in the photoreaction, where A_0 is time-independent; A_1 and A_2 are time-dependent components. However, as all of them are describing the same reaction, part A_0 also exhibits little time-dependency especially at the early stages of the reaction.

As given in Table 1, A_1 and A_2 provide the rate constants k_1 and k_2 , showing the fast and slow parts A_1 and A_2 , respectively. The presence of such a fast time-dependency character strongly indicates that it is coming from the excimer, which can be disintegrating into the stable dimer phase. This is in agreement with reports on the monomer–dimer transformations due to the photoreaction, where the excimer either decays to stable monomers or forms a dimer phase. Forming the excimer state was found to be faster than forming the stable dimer (Takegoshi *et al.*, 1998; Ferguson & Mau, 1974), and it has been reported that the excimer phase is unstable at room temperature (Horiguchi *et al.*, 1987).

The appearance of the slower component A_2 is also compatible with the reported literature for the mechanism of photodimerization, where the photodimerization mechanism involves a slow process forming a stable dimer in addition to a faster one for the metastable state (excimer) (Birks &

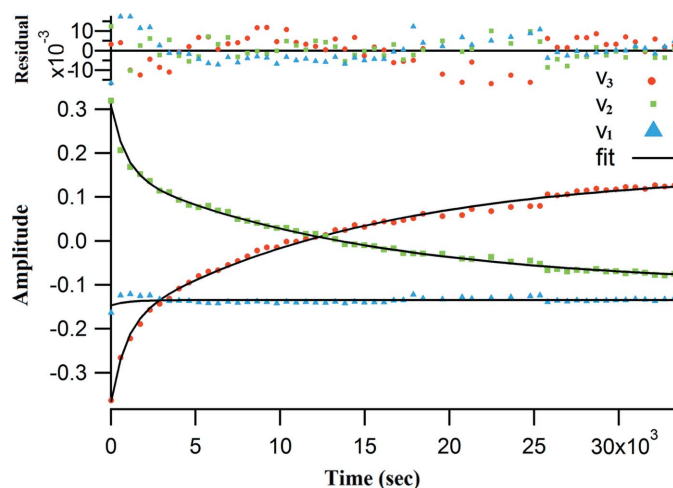


Figure 10
Plot of global fitting results of the time-dependent V spectra for 9-MA SVD analysis. A residual plot shows the residuals of v_1 , v_2 and v_3 on the vertical axis and the independent variable on the horizontal axis.

Aladekomo, 1963; Takegoshi *et al.*, 1998; Ferguson & Mau, 1974).

A more detailed discussion about photoisomerization kinetics and the phase growth mechanism of 9-MA has been given by Mabied *et al.* (2012). The dimer peaks were distinguished and could be analyzed using Rietveld refinement after about 30 min from the beginning of the reaction (Fig. 1). However, the dimer and its associated excimer state should exist at the start of the reaction and could enhance the change of the average diffraction intensity in the monomer phase even though the dimer peaks have not yet appeared. In the present work, SVD has treated all of the time-dependent data sets from the start of the reaction showing traces to the excimer state; such a way of data treatment may also cause the variation of the numerical magnitude of the rate constants between the reported growth rate (Mabied *et al.*, 2012) and the present study (Table 1). Similar ($4\pi+4\pi$) photodimerization studies have reported rate constants with similar orders of the numerical results, $k = 9.7 (14) \times 10^{-8} \text{ s}^{-1}$ and $k = 2.1 (26) \times 10^{-6} \text{ s}^{-1}$ (Cao *et al.*, 2010).

The UV–Vis and IR spectra supported the SVD analysis results of 9-MA. The IR spectrum showed the appearance of the aliphatic C–H saturated bond for the dimer phase (Fig. 8*a*) below 3000 cm^{-1} (Singh & Sandorfy, 1969). The absorption peaks between 350 and 400 nm (Fig. 8*b*) disappeared in the UV–Vis spectrum of the illuminated 9-MA, which was reported as an indication of the formation of the dimer phase (Tillman *et al.*, 2007).

5. Conclusions

SVD analysis for time-resolved powder diffraction of photodimerization reactions was introduced in order to effectively extract meaningful parameters from a small amount of changes from the time-dependent crystallographic data. 1-chA and 9-MA were successful examples of SVD application to the analysis of time-dependent powder diffraction experiments.

The results of SVD analysis revealed significant information of 9-MA and 1-chA photodimerization, which strongly suggest the existence of the excimer state even if it is difficult to detect directly, and supported the formation of the 9-MA stable dimer phase.

SVD analysis of time-dependent powder diffraction experiments can be recommended as a powerful tool discovering the important features hidden in their data sets, which leads to more useful applications. Using visualization methods, in addition to considering the physical description of the model under study and global fitting, is a very helpful method for investigation of the results.

The synchrotron X-ray experiment at KEK was approved by the Photon Factory Program Advisory Committee (PF-PAC No. 2004S2-001). This work was partly supported by the Asia–Africa Science Platform Program by JSPS. We thank Dr Michael Cheah [Australian National Beamline Facility (ANBF), KEK, Japan] for his help with the spectroscopic measurements.

References

- Aladekomo, J. (1973). *J. Lumin.* **6**, 83–95.
- Alter, O., Brown, P. O. & Botstein, D. (2000). *Proc. Natl Acad. Sci.* **97**, 10101–10106.
- Berlich, A., Liu, Y. C. & Morgner, H. (2005). *Radiat. Phys. Chem.* **74**, 201–209.
- Birks, J. B. & Aladekomo, J. B. (1963). *Photochem. Photobiol.* **2**, 415–418.
- Bouas-Laurent, H., Desvergne, J.-P., Castellan, A. & Lapouyade, R. (2001). *Chem. Soc. Rev.* **30**, 248–263.
- Cao, D. K., Sreevidya, T. V., Botoshansky, M., Golden, G., Benedict, J. B. & Kaftory, M. (2010). *J. Phys. Chem. A*, **114**, 7377–7381.
- Cattell, R. B. (1966). *Multivar. Behav. Res.* **1**, 245–276.
- Dvornikov, A. S. & Rentzepis, P. M. (1996). *Res. Chem. Intermed.* **22**, 115–128.
- Ferguson, J. & Mau, A.-H. (1974). *Mol. Phys.* **27**, 377–387.
- Golub, G. & Van Loan, C. (1996). *Matrix Computations, Johns Hopkins Studies in the Mathematical Sciences*. Johns Hopkins University Press.
- Hammersley, A. P., Svensson, S. O., Hanfland, M., Fitch, A. N. & Hausermann, D. (1996). *High Press. Res.* **14**, 235–248.
- Henry, E. R. (1997). *Biophys. J.* **72**, 652–673.
- Henry, E. & Hofrichter, J. (1992). *Numerical Computer Methods*, edited by M. L. J. Ludwig Brand, Vol. 210 of *Methods in Enzymology*, pp. 129–192. New York: Academic Press.
- Hinrichsen, B., Dinnebier, R. E. & Jansen, M. (2006). *Z. Kristallogr. Suppl.* **23**, 231–236.
- Horiguchi, R., Iwasaki, N. & Maruyama, Y. (1987). *J. Phys. Chem.* **91**, 5135–5139.
- Lahabar, S. & Narayanan, P. (2009). *Parallel Distributed Processing 2009, IEEE International Symposium on IPDPS 2009*, pp. 1–10.
- Mabied, A. F., Müller, M., Dinnebier, R. E., Nozawa, S., Hoshino, M., Tomita, A., Sato, T. & Adachi, S. (2012). *Acta Cryst.* **B68**, 424–430.
- Molard, Y., Bassani, D. M., Desvergne, J.-P., Moran, N. & Tucker, J. H. R. (2006). *J. Org. Chem.* **71**, 8523–8531.
- Nozawa, S., Adachi, S., Takahashi, J., Tazaki, R., Guérin, L., Daimon, M., Tomita, A., Sato, T., Chollet, M., Collet, E., Cailleau, H., Yamamoto, S., Tsuchiya, K., Shioya, T., Sasaki, H., Mori, T., Ichianagi, K., Sawa, H., Kawata, H. & Koshihara, S. (2007). *J. Synchrotron Rad.* **14**, 313–319.
- Oka, T., Yagi, N., Fujisawa, T., Kamikubo, H., Tokunaga, F. & Kataoka, M. (2000). *Proc. Natl Acad. Sci. USA*, **97**, 14278–14282.
- Okamoto, S. & Sakurai, S. (2003). *J. Appl. Cryst.* **36**, 982–985.
- Rajagopal, S., Schmidt, M., Anderson, S., Ihee, H. & Moffat, K. (2004). *Acta Cryst.* **D60**, 860–871.
- Roissnel, T. & Rodriguez-Carvajal, J. (2001). *Mater. Sci. Forum*, **378–381**, 118–123.
- Schmidt, G. M. J. (1971). *Pure Appl. Chem.* **27**, 647–678.
- Singh, S. & Sandorfy, C. (1969). *Can. J. Chem.* **47**, 257–263.
- Stoer, J. & Bulirsch, R. (2002). *Introduction to Numerical Analysis. Texts in Applied Mathematics*. Berlin: Springer.
- Takegoshi, K., Nakamura, S. & Terao, T. (1998). *Solid State Nucl. Magn. Res.* **11**, 189–196.
- Tillman, E. S., Miller, D. J. & Roof, A. C. (2007). *Polym. Bull.* **58**, 881–891.
- Unonius, L. & Paatero, P. (1990). *Comput. Phys. Commun.* **59**, 225–243.
- Van Wilderen, L. J. G. W., Lincoln, C. N. & van Thor, J. J. (2011). *PLoS ONE*, **6**, e17373.
- Wall, M., Rechtsteiner, A. & Rocha, L. (2003). *A Practical Approach to Microarray Data Analysis*, pp. 91–109. Kluwer: Norwell.
- Wave Metrics (2011). *IGOR Pro 6.22 User's Manual: Technical graphing and data analysis software for scientists and engineers*.
- Zhang, L., Quan, D., Wang, L., Yang, G. & Weng, Y. (2004). *Sci. Chin. Ser. G: Phys. Mech. Astron.* **47**, 208–222.
- Zhao, P., Fang, C. F., Xia, C. J. M. W. Y., Liu, D. S. & Xie, S. J. (2008). *Appl. Phys. Lett.* **93**, 013113.
- Zhao, Y. & Schmidt, M. (2009). *J. Appl. Cryst.* **42**, 734–740.